Metal–Organic Frameworks

DOI: 10.1002/anie.201101534

Functional Mixed Metal–Organic Frameworks with Metalloligands

*Madhab C. Das, Shengchang Xiang, Zhangjing Zhang, and Banglin Chen**

drug delivery · heterogeneous catalysis · metal–organic frameworks · sensors · separation procedures

Immobilization of functional sites within metal–organic frameworks (MOFs) is very important for their ability to recognize small molecules and thus for their functional properties. The metalloligand approach has enabled us to rationally immobilize a variety of different functional sites such as open metal sites, catalytic active metal sites, photoactive metal sites, chiral pore environments, and pores of tunable sizes and curvatures into mixed metal–organic frameworks (M′MOFs). In this Minireview, we highlight some important functional M′MOFs with metalloligands for gas storage and separation, enantioselective separation, heterogeneous asymmetric catalysis, sensing, and as photoactive and nanoscale drug delivery and biomedical imaging materials.

1. Introduction

The emergence of functional coordination polymer (CP) and metal–organic framework (MOF) materials has been one of the most significant achievements in the inorganic and materials science community over the past two decades.[1] Such frameworks can be readily self-assembled from metal ions or metal-containing clusters (generally termed secondary building units (SBUs)) with organic linkers through metal–organic-linker coordination bonds. Because the metal ions and clusters can have certain preferred coordination geometries, self-assembly of these moieties (generally termed as nodes) with organic linkers (connectors) of predetermined shapes can lead to the construction of metal–organic frameworks with predictable structures. For example, the $\{Zn_4O(COO)_6\}$ clusters as six-coordinate nodes connect with the linear bicarboxylates $L^1(COO)_2$ (L^1 = ligand) to form the MOFs $[Zn_4O(L^1(COO)_2)_3]$ of the default cubic structures.[2] Such a so-called rational design or reticular synthesis approach is very important to synthesize microporous MOFs of predictable structures and thus with tunable pore sizes and curvatures, which are important for their properties, particularly for gas storage and separation. In fact, a variety of porous MOFs of diverse structures and topologies have been realized and applied for gas storage and separation of small gas molecules such as hydrogen, methane, carbon dioxide, acetylene and ethylene.

Immobilization of functional sites such as open metal sites and Lewis acidic and basic sites for their specific and selective recognition of guest substrates within porous MOFs has played a crucial role in the development of functional MOFs for their applications in gas storage and separation, heterogeneous catalysis, sensing, and drug delivery.[1] One general methodology to immobilize functional sites in porous MOFs is to make use of organic linkers with organic groups such as NH_2, OH, and SO_3H. For example, the microporous MOF with the terminal NH_2 groups immobilized on the pore surfaces has been revealed to bind CO_2 strongly and enforces the highly selective separation of CO_2 from N_2.[3] As for the construction of open metal sites within traditional porous MOFs, although extensive research has been devoted to this task and the very important roles of such open metal sites for their gas storage, separation, heterogeneous catalysis, and sensing has been realized, only a few types of porous MOFs with open metal sites in the nodes could be systematically targeted before the exploration of metalloligand approach. One type of porous MOF in which the open metal sites can be rationally generated is those MOFs assembled from the paddle-wheel cluster $\{Cu_2(COO)_4(solvent)_2\}$ with carboxylates. The release of the terminal solvent molecules from the paddle-wheel cluster $\{Cu_2(COO)_4(solvent)_2\}$ nodes through thermal and vacuum activation has led to a series of $\{Cu_2(COO)_4\}$-containing porous MOFs with open Cu^{2+} sites for storage of hydrogen, acetylene, and methane. Because of the

[*] Dr. M. C. Das, Dr. S. Xiang, Dr. Z. Zhang, Prof. Dr. B. Chen
Department of Chemistry
University of Texas at San Antonio
San Antonio, Texas 78249-0698 (USA)
Fax: (+1) 210-458-7428
E-mail: banglin.chen@utsa.edu

unique roles of the functional sites for the properties of such porous materials, it is very important to develop new methodologies to systematically immobilize functional sites in porous MOFs. In this regard, the metalloligand approach is certainly one of the most promising ones. As shown in Scheme 1, instead of pure organic linkers in the construction of traditional MOFs, metal–organic complexes as the metalloligands are utilized to coordinate with the second metal ions or metal clusters (M′) to form the so-called mixed metal–organic frameworks (M′MOFs). Such a metalloligand approach can not only readily generate tunable pore sizes and curvatures and chiral pore environments (by making use of chiral metalloligands) but can also rationally immobilize different metal sites such as open metal sites, catalytically active metal sites, and photoactive metal sites into the porous M′MOFs for their functional properties.

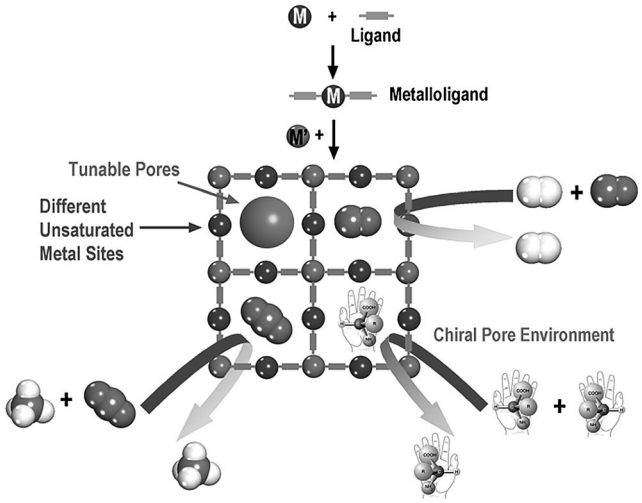

Scheme 1. The metalloligand approach to construct mixed metal–organic frameworks (M′MOFs).

Madhab C. Das was born in Midnapore, West Bengal, India. He received his B.S. (2002) from Midnapore College and M.S. (2004) from Vidyasagar University in India. He then moved to the Indian Institute of Technology (IIT) Kanpur where he received his Ph.D. in supramolecular chemistry under the supervision of Professor Parimal K. Bharadwaj in November 2009. Since December 2009 he has been working with Professor Banglin Chen at the University of Texas at San Antonio as a postdoctoral fellow. His work is focused on functional metal–organic frameworks.

Shengchang Xiang was born in Fujian, China (1972) and received his Ph.D. degree in physical chemistry in 2003 from Fuzhou University. He joined in Prof. Xin-Tao Wu's group at the Fujian Institute of Research on the Structures of Matter, Chinese Academy of Sciences, as a postdoctoral Fellow and then associate professor (2003–2007). He is now working at the University of Texas at San Antonio as a postdoctoral fellow with Prof. Banglin Chen. His work is focused on multifunctional organic–inorganic hybrid materials.

$[Cu^{II}(tpp)]$ (tpp = 5,10,15,20-tetra(4-pyridyl)-21*H*,23*H*-porphine) and $[Cu^{II}(tcp)]$ (tcp = 5,10,15,20-tetra(4-cyanophenyl)-21*H*,23*H*-porphine) might have been the first two metalloligands utilized to construct coordination polymers $[Cu^{II}(tpp)Cu^{I}]BF_4$ and $[Cu^{II}(tcp)Cu^{I}]BF_4$.[4] However, these two frameworks were not robust enough to retain the porous structures once the solvent molecules were removed from the pore cavities, apparently because of the flexible nature of the coordination geometry of Cu^{I}. A few metalloligands containing pba (1,3-propylenebis(oxamato)), opba (o-phenylenebis(oxamato)), or opb (oxamido-bis(propionato)) chelating moieties were developed and incorporated into hetero- or bimetallic magnetic coordination polymers during 1980s.[5] Kosal et al. realized the first stable Co-CoT(*p*-CO_2)PP framework $[CoT(p\text{-}CO_2)PPCo_{1.5}]$ (PIZA-1; T(*p*-CO_2)PP = 5,10,15,20-tetra(*p*-carboxyphenylporphyrinate)) by making use of porphyrin tetracarboxylates.[6] To incorporate a phosphonic acid substituted Ru-binap-dpen metalloligand building block (binap = 2,2′-bis(diphenylphosphanyl)-1,1′-binaphthyl) into a chiral porous zirconium phosphonate framework, Hu et al. synthesized an amorphous porous framework $Zr[Ru(L^2)(dpen)Cl_2]\cdot 4H_2O$ (H_4L^2 = (*R*)-2,2′-bis(diphenylphosphino)-1,1′-binaphthyl-4,4′-bis(phosphonic acid; dpen = 1,2-diphenylethylenediamine) for heterogeneous asymmetric hydrogenation of aromatic ketones.[7b] Kitaura et al. and Chen et al. utilized the metalloligands $[Cu(H_2salphdc)]$ (H_4salphdc = *N*,*N*′-phenylenebis(salicylideneimine)dicarboxylic acid) and $[Cu(Pyac)_2]$ (Pyac = 3-(4-pyridyl)pentane-2,4-dionato) to construct several crystalline M′MOFs, which have initiated the renewed interest in the construction of mixed metal–organic frameworks, particularly crystalline functional M′MOFs (Scheme 2).[8,9] Over the past several years, a series of such M′MOFs have been realized exhibiting permanent porosity for small-gas separation, asymmetric catalysis, chemical sensing, and as photoactive, luminescent, and nanoscale drug delivery and biomedical imaging materials.[10–31] This Minireview highlights some important functional mixed metal–organic framework (M′MOF) materials.

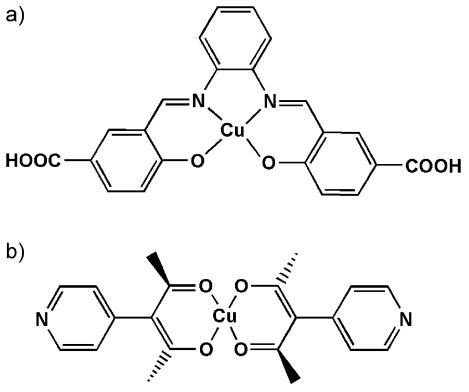

Scheme 2. The metalloligands a) $Cu(H_2salphdc)$ and b) $Cu(Pyac)_2$.[8,9]

2. Functional M′MOFs for Gas Storage and Separation

Our group is now focused on the construction of microporous M′MOFs with rationally immobilized open metal sites for gas storage and separation.[10,11] We have shown that in the first step, a Cu^{II} Schiff base complex in the form of the metalloligand building block {Cu(Pyen)} could be readily achieved via the condensation of corresponding aldehyde and ethylenediamine and further complexation with $Cu(NO_3)_2$.[10] This metallo-Schiff base contains two free terminal pyridine moieties available for binding with other metal ions for the second step reaction (Figure 1Ia). A solvothermal reaction among $[Cu(H_2Pyen)](NO_3)_2$, benzene-1,4-dicarboxylic acid (H_2bdc), and $Zn(NO_3)_2$ led to the formation of $[Zn_3(bdc)_3Cu(Pyen)(G)_x]$ (M′MOF **1;** G = guest molecules). The framework is composed of trinuclear $\{Zn_3(COO)_6\}$ SBUs (Figure 1Ib). These SBUs are bridged by bdc moieties to form 3^6 tessellated $\{Zn_3(bdc)_3\}$ 2D sheets (Figure 1Ic) that are further pillared by the {Cu(Pyen)} units to build the 3D network. The rationally immobilized Cu centers reside within two types of micropores (curved pores and irregular ultra-micropores along *c* and *b* directions, respectively; Figure 1Id,e), which interact with H_2 molecules through two open metal sites per copper atom with an enthalpy of $(12.29 \pm 0.53)\ kJ\,mol^{-1}$ at zero coverage (Figure 1II). The most significant feature was the differential adsorption kinetics for H_2 and D_2 (Figure 1III). The rate constant for D_2 was higher but the activation energy was slightly lower compared to the corresponding values for H_2. The higher effective collision cross-section of H_2, because of the higher zero-point energy, produced a higher barrier to diffuse through the open pores than for D_2.[32] Thus it was possible to obtain the first experimental evidence of kinetic isotope quantum molecular sieving in such microporous M′MOF materials.

This success has encouraged us to construct a series of isoreticular M′MOFs in which the micropores can be tuned and functionalized by a variety of the following strategies:

a) Incorporation of different secondary organic linkers such as *trans*-1,4-cyclohexanedicarboxylic acid, 4,4′-biphenyldicarboxylic acid, and 2,6-napthalenedicarboxylic acid.
b) Immobilization of metal centers other than copper(II) within the metal Schiff base metalloligands.
c) Incorporation of chiral pockets/environments by using different chiral diamines.
d) Use of different derivatives of the pyridyl donor moiety such as *tert*-butyl, phenyl, and cyclohexyl instead of the methyl group.
e) Incorporation of metal ions other than zinc(II) as the nodes for M′MOFs.

A combination of strategies a and c led to the formation of two isostructural M′MOFs in which the micropores are rationally tuned and functionalized to show enantioselectivity towards small alcohols and highly selective separation of acetylene over ethylene.[11]

As shown in Scheme 3, chiral (*R*,*R*)-1,2-cyclohexanediamine was used to construct the preorganized chiral metalloligand [Cu(SalPyCy)]. The metalloligand [Cu(SalPyCy)] was treated with either H_2bdc or H_2cdc (H_2cdc = *trans*-1,4,-cyclohexanedicarboxylic acid) along with Zn^{II} under solvothermal conditions to construct $[Zn_3(bdc)_3\{Cu(SalPyCy)\}(G)_x]$ (**2**) and $[Zn_3(cdc)_3\{Cu(SalPyCy)\}(G)_x]$ (**3**) with isostructural 3D frameworks. Amazingly, the subtle tuning of the micropores by the change of bdc in **2** to cdc in **3** led to significantly enhanced C_2H_2/C_2H_4 separation at both 195 and 295 K for the activated M′MOF $[Zn_3(cdc)_3\{Cu(SalPyCy)\}]$ (**3a**) (Figure 2).[11]

$[Cu(Pyac)_2]$ is a versatile metalloligand to synthesize different M′MOFs (Scheme 2b).[8,9] Sakamoto et al. reported a M′MOF $[\{Cu_2(pzdc)_2Cu(Pyac)_2H_2O^b\}\cdot 4H_2O^c]_n$ (H_2O^b = bound water, H_2O^c = water of crystallization, Na_2pzdc = disodium 2,3,-pyrazinedicarboxylate) having active metal sites generated through the complementary coordination-bond rearrangement. The resulting framework retained its permanent porosity, as confirmed by N_2, O_2, CO_2, H_2O, MeOH, and EtOH sorptions (Figure 3).[8b]

Bloch et al. demonstrated insertion of metal ions into a microporous MOF material lined with 2,2′-bipyridine moieties to construct microporous M′MOFs (Figure 4a).[12] Both palladium(II) and copper(II) sites can be immobilized in the pores of the resulting M′MOFs. The microporous M′MOF $[Al(OH)(bpydc)][Cu(BF_4)_2]_{0.97}$ exhibits much higher CO_2/N_2 selectivity (12) compared with the original MOF [Al(OH)(bpydc)] (2.8), because of the immobilization of copper sites on the pore surfaces and the reduced pores (Figure 4b).

Zhangjing Zhang earned her PhD in 2007 from Fujian Institute of Research on the Structure of Matter, Chinese Academy of Sciences, under the direction of Prof. Guocong Guo. She worked with Prof. Paul Maggard before joining the University of Texas at San Antonio in 2009 as a postdoctoral fellow with Prof. Banglin Chen. Her research is related to metal–organic supramolecules and frameworks for applications in gas storage and separations, as sensors, in catalysis, and for electronics and devices.

Banglin Chen was born in Zhejiang, China. He received B.S. (1985) and M.S. (1988) degrees in chemistry from Zhejiang University in China and his Ph.D. from the National University of Singapore in 2000. He worked with Professors Omar M. Yaghi at the University of Michigan, Stephen Lee at Cornell University, and Andrew W. Maverick at Louisiana State University as a postdoctoral fellow (2000–2003) before joining the University of Texas–Pan American in 2003. He moved to the University of Texas at San Antonio in August 2009, where he is now Professor of Chemistry.

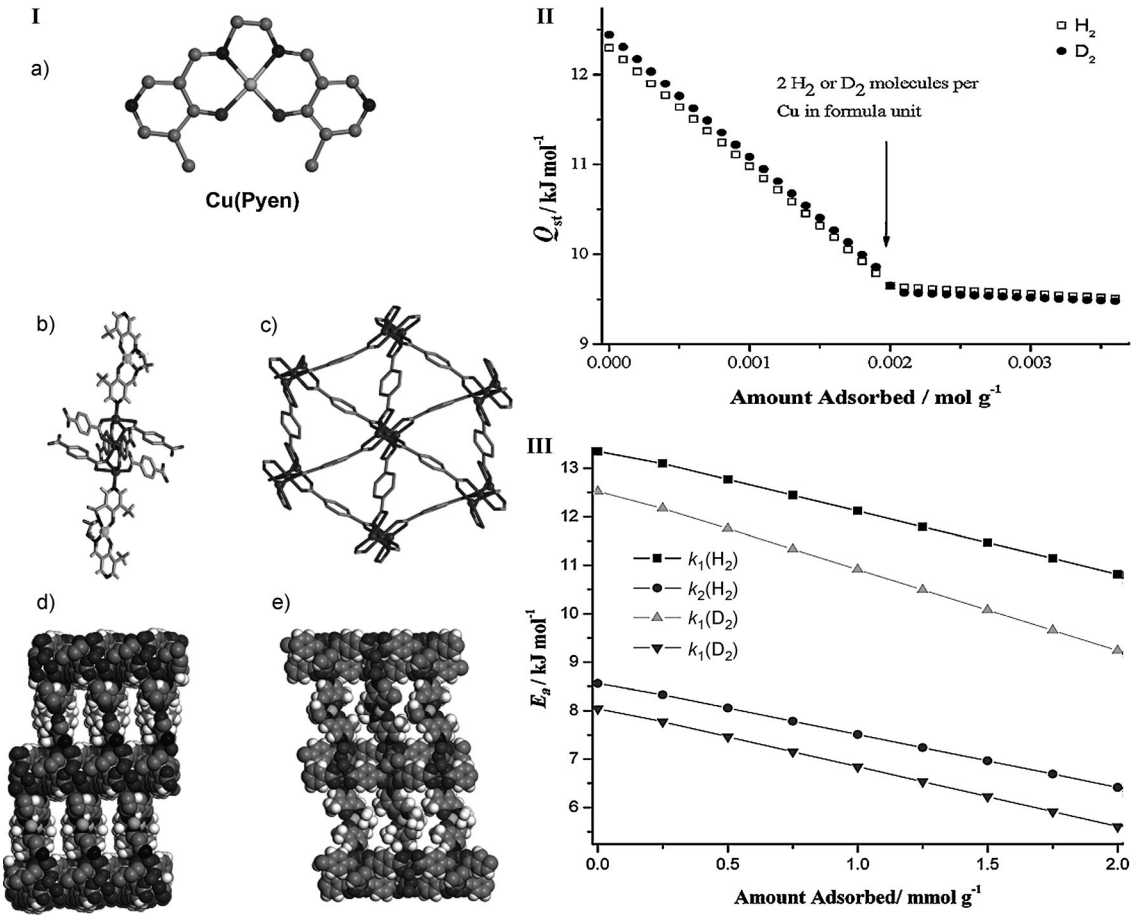

Figure 1. I. X-ray crystal structure of M′MOF **1** ($[Zn_3(bdc)_3Cu(Pyen)]$) showing a) Pyen, b) one trinuclear $\{Zn_3(COO)_6\}$ SBU, c) one 3^6 tessellated $\{Zn_3(bdc)_3\}$ 2D sheet that is pillared by the {Cu(Pyen)} units to form a 3D microporous M′MOF **1** having d) curved pores with dimensions of about 5.6×12.0 Å^2 along the *c* axis and e) irregular ultramicropores along the *b* axis. II. The variation of enthalpy of adsorption (isosteric heat of adsorption Q_{st} in kJ mol^{-1}) with amount (mol g^{-1}) of adsorbed H_2 and D_2 on M′MOF **1**. III. The variation of activation energy (E_a in kJ mol^{-1}) with amount (mmol g^{-1}) of adsorbed H_2 and D_2 on M′MOF **1**, where k_1 and k_2 are diffusion rate constants. Reproduced with permission from Ref. [10].

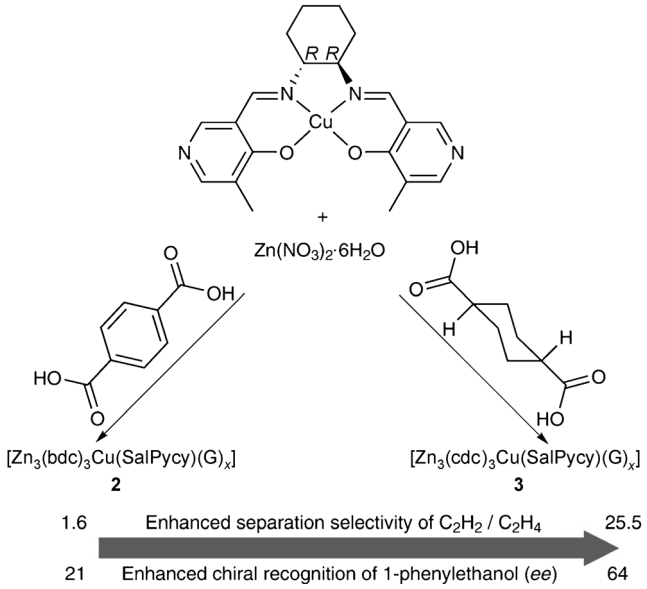

Scheme 3. Metalloligand approach for the construction of two M′MOFs (**2** and **3**). M′MOF **3** shows better C_2H_2/C_2H_4 gas separation and chiral alcohol separation than **2**. Reproduced with permission from Ref. [11].

3. Functional M′MOFs for Size, Shape, and Enantioselective Separation of Small Organic Molecules

Kosal et al. reported a M′MOF (PIZA-1) assembled from metalloporphyrins in which Co^{III} porphyrin cores were connected by bridging trinuclear Co^{II} carboxylate clusters (Figure 5a).[6] The robustness and integrity of the activated material was confirmed by PXRD and N_2 adsorption measurements. Size and shape selectivity for different guest molecules were studied by thermal desorption, in which the adsorbed guest molecules were desorbed at elevated temperatures to examine the uptake amount and thus to compare the selectivity. For example, PIZA-1 takes up less aromatic amine when the size of the guest aromatic amine increases; while the selectivity for linear alkyl amines ($C_nH_{2n+1}NH_2$) is dependent on the chain length, in which short-chain amines ($n=4$–6) were preferably adsorbed over their long-chain ($n=7$–10) counterparts (Figure 5b).

The M′MOFs **2** and **3** have been used for chiral recognition and chiral separation of the small alcohol 1-phenylethanol (PEA).[11] The achiral M′MOF **1** encapsulated

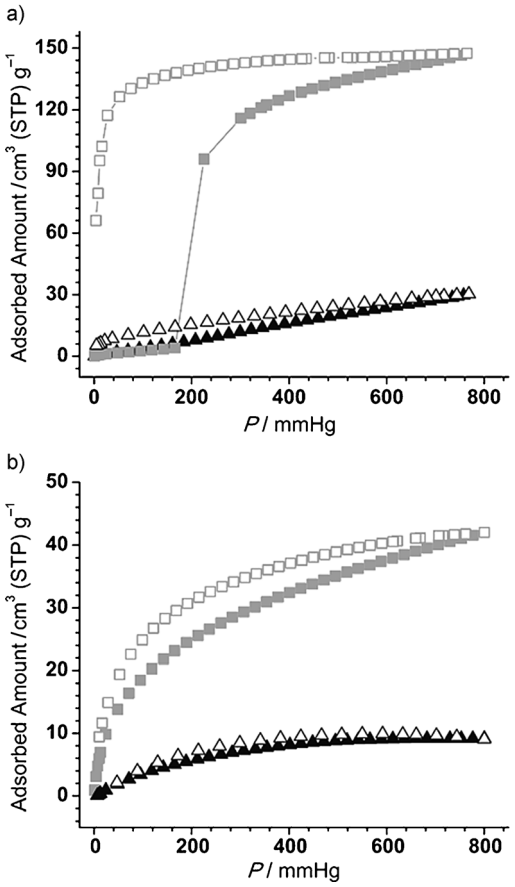

Figure 2. Adsorption (solid symbols) and desorption (open symbols) isotherms of acetylene (squares) and ethylene (triangles) on **3a** at a) 195 K and b) 295 K. STP = standard temperature and pressure. Reproduced with permission from Ref. [11].

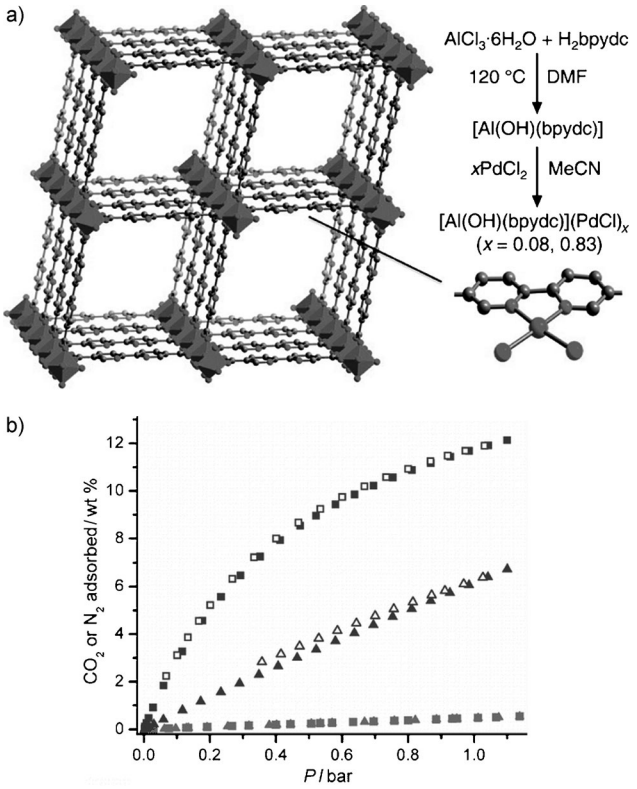

Figure 4. a) Synthesis and representative structure of [Al(OH)(bpydc)], with subsequent insertion of $PdCl_2$ into bpydc ligand sites. b) Adsorption isotherms of CO_2 in [Al(OH)(bpydc)] (black triangles) and [Al(OH)(bpydc)][$Cu(BF_4)_2$]$_{0.97}$ (black squares) and N_2 in [Al(OH)(bpydc)] (gray triangles) and [Al(OH)(bpydc)][$Cu(BF_4)_2$]$_{0.97}$ (gray squares). Filled and open symbols represent adsorption and desorption, respectively. Reproduced with permission from Ref. [12].

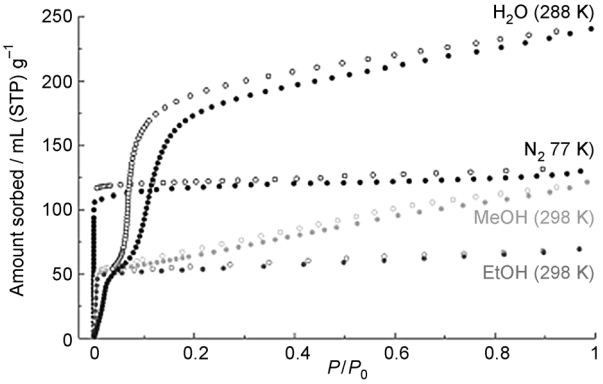

Figure 3. Sorption isotherms of N_2 at 77 K, H_2O at 288 K, MeOH at 298 K, and EtOH at 298 K for dehydrated M′MOF [Cu_2(pzdc)$_2$Cu(Pyac)$_2$]. Reproduced with permission from Ref. [8b].

both (*R*)- and (*S*)-PEA into its channels, as confirmed by single-crystal X-ray analysis. In comparison, **3** exclusively took up (*S*)-PEA in its cavity, thus showing its potential for chiral recognition (Figure 6) of small alcohols. The HPLC analysis showed an uptake of (*S*)-PEA with an *ee* value of 21.1% (15.7 and 13.2% for second and third regenerated samples, respectively) for **2**, whereas this value increases to 64% for **3** (55.3 and 50.6% for second and third regenerated samples, respectively). This result was attributed to the smaller pore sizes of **3** compared to **2**, which significantly enhanced the enantioselectivity.

A homochiral lamellar solid could be self-assembled from an unsymmetrical Schiff base ligand with one pendent carboxylate moiety and copper(II) nitrate.[13] The ligand used one tridentate N_2O donor site to bind one copper(II) center and one monodentate carboxylate group to bind another copper(II) center to form an H-bonded chiral helical layered structure. This M′MOF showed enantioselective recognition and separation of racemic secondary alcohols with excellent enantiomeric excess greater than 99.5%.

4. Functional M′MOFs as Heterogeneous Asymmetric Catalysts

From the very beginning of the MOF field, it was a dream to use a MOF for selective heterogeneous catalysis. Asymmetric hydrogenation is considered as one of the most efficient strategies to synthesize optically active molecules. The ruthenium and rhodium complexes of binap were found to be very effective for the reduction of a wide range of

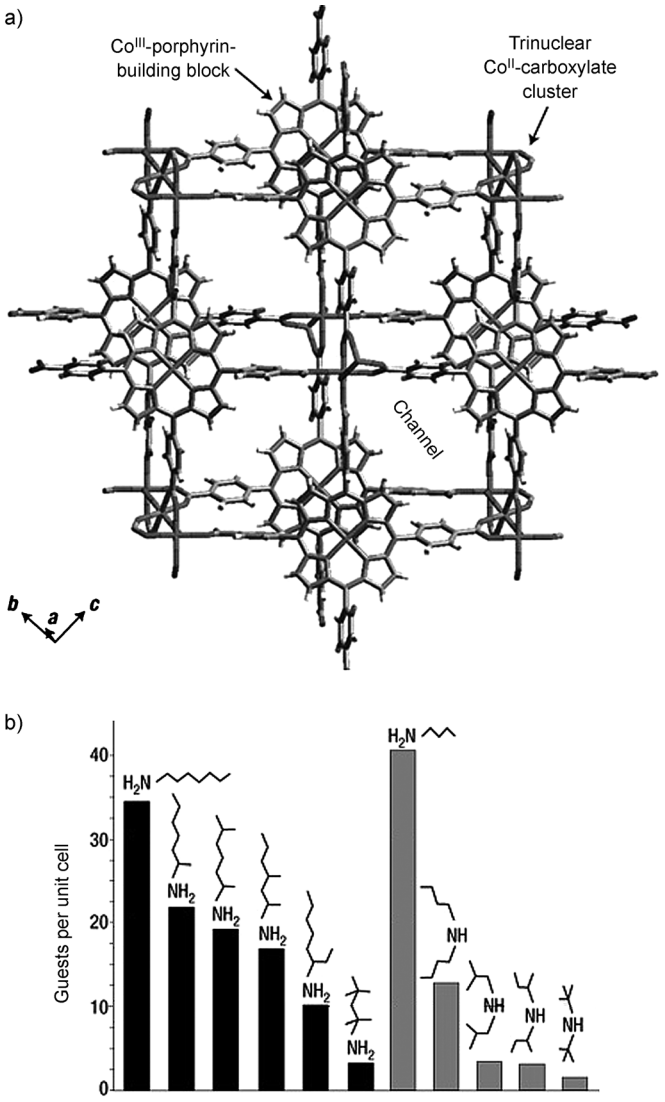

Figure 5. a) X-ray structure of PIZA-1 viewed along the *a* axis showing connectivity leading to formation of 13.8×6.8 Å^2 channels. b) Selectivity observed in a variety of chemicals by PIZA-1. Reproduced with permission from Ref. [6].

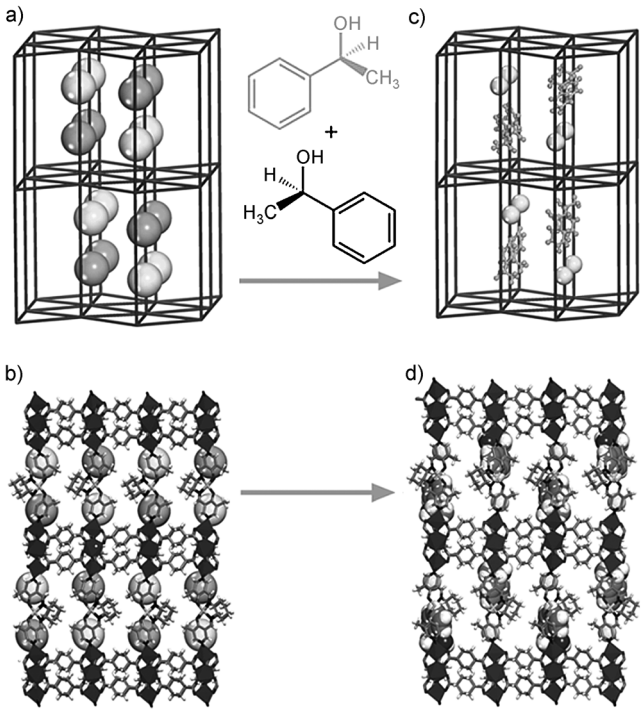

Figure 6. Left: X-ray crystal structures of **3** showing a) the hexagonal primitive network topology and b) the 3D pillared framework with chiral cavities. Right: **3** with encapsulated (*S*)-PEA showing c) the hexagonal primitive network topology and d) the 3D pillared framework exclusively encapsulating (*S*)-PEA molecules. Reproduced with permission from Ref. [11].

substrates with high enantioselectivity, but practical industrial applications were often hindered by the high costs and the difficulty in removing leached toxic metals from the organic products.[33] To address these problems, Hu et al. successfully synthesized chiral porous zirconium phosphonates containing Ru binap moieties for enantioselective heterogeneous asymmetric hydrogenation of β-keto esters (Scheme 4).[7a] The enatiopure metalloligands $[Ru(H_4L^3)(dmf)_2Cl_2]$ (H_4L^3 = 2,2'-bis(diphenylphosphanyl)-1,1'-binaphthyl-6,6'-bis(phosphonic acid)) and $[Ru(H_4L^2)(dmf)_2Cl_2]$ were self-assembled with zirconium salt to form two chiral porous M′MOFs **4** and **5**. M′MOF **4** exhibited a total BET surface area[34] of 475 m^2g^{-1} with pore volume of 1.02 cm^3g^{-1}, while these values were 387 m^2g^{-1} and 0.53 cm^3g^{-1} for **5**. M′MOF **4** was found to catalyze hydrogenation of a wide range of β-alkyl-substituted β-keto esters with complete conversions. The *ee* values ranged from 91.7 to 95.0%, comparable to the homogeneous Ru binap catalyst. This system showed an excellent recyclability for as many as five cycles with complete conversions and high *ee* values.

A slight modification of the ruthenium-containing metalloligands by incorporation of chelating ligand such as dpen and subsequent complexation with zirconium salt resulted in

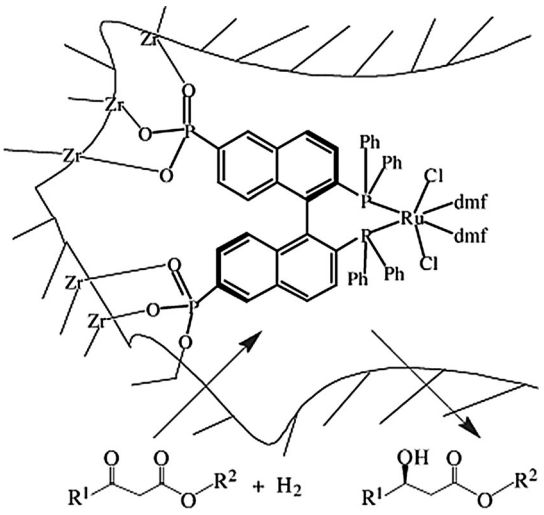

Scheme 4. Schematic representation of chiral M′MOF **4** showing heterogeneous asymmetric hydrogenation of β-keto esters. Reproduced with permission from Ref. [7a].

another two chiral porous M′MOFs, which showed excellent enantioselective heterogeneous asymmetric hydrogenation of aromatic ketones.[7b] A 0.1 mol% loading of 4,4′-disubstituted binap M′MOF was found to catalyze a series of aromatic ketones to their corresponding alcohols with remarkably high *ee* values of 90.6–99.2% and complete conversions, which were significantly higher than those observed for the parent Ru binap dpen homogeneous catalyst.

A chiral microporous M′MOF $[Zn_2(bpdc)_2L^4]\cdot 10DMF\cdot 8H_2O$ ($L^4 = (R,R)$-(2)-1,2-cyclohexanediamino-*N*,*N*′-bis(3-*tert*-butyl-5-(4-pyridyl)salicylidene)$Mn^{III}Cl$) reported by Cho et al. was used as an enatioselective catalyst for olefin epoxidation.[14] A solvothermal reaction between a manganese salen-type metalloligand unit with Zn^{II} and 4,4′-biphenyldicarboxylic acid led to the formation of this novel M′MOF of doubly interpenetrated α-polonium net (Figure 7).

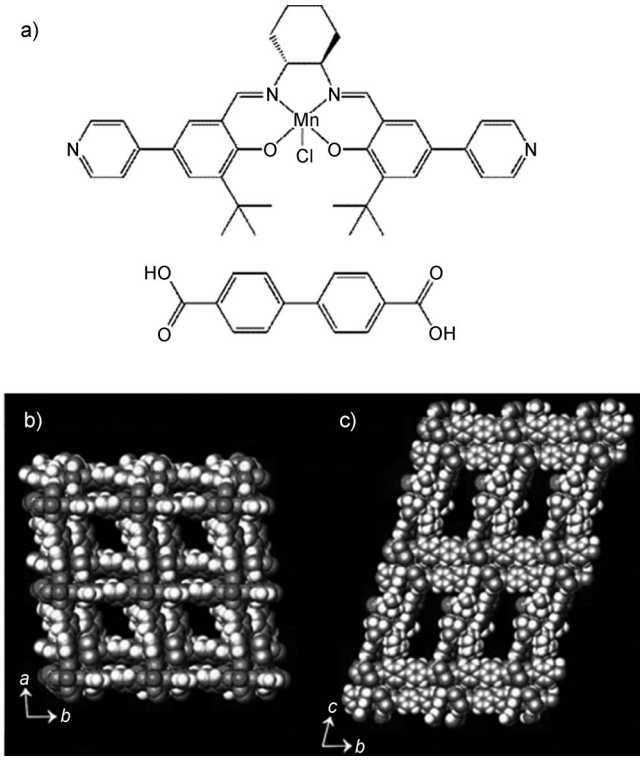

Figure 7. a) Representation of manganese salen-type metalloligand L^4 and 4,4′-biphenyldicarboxylic acid (H_2bpdc). b) Space-filling representation of $[Zn_2(bpdc)_2L^4]\cdot 10DMF\cdot 8H_2O$ showing interpenetrating networks and c) framework openings viewed down crystallographic *c* and *a* axes, respectively. Reproduced with permission from Ref. [14].

This M′MOF was thermally stable up to 360 °C, and the activated sample retained its crystallinity, thus making it useful to examine its catalytic activity towards asymmetric epoxidation of 2,2-dimethyl-2*H*-chromene in presence of an oxidant. This M′MOF showed only minor selectivity degradation with 82% *ee* (88% *ee* for the free metalloligand L^4) because of the electronic effect arising from binding of pyridyl groups to zinc cations, but had no loss of enantioselectivity and a small loss of activity even after three cycles. The recyclability, easy separation, and extended catalyst lifetime certainly makes this M′MOF a better catalyst than the free metalloligand L^4.[14]

Recently, Song et al. reported a family of isoreticular chiral M′MOFs of primitive cubic network topology for asymmetric alkene epoxidation.[15] Five M′MOFs with tunable open channels were synthesized by direct incorporation of three different chiral manganese salen subunits of varied lengths, exhibiting non-interpenetrating frameworks for **7** and **9** and two- or threefold interpenetrating frameworks for **6**, **8**, and **10** (Figure 8). These M′MOFs were shown to be highly

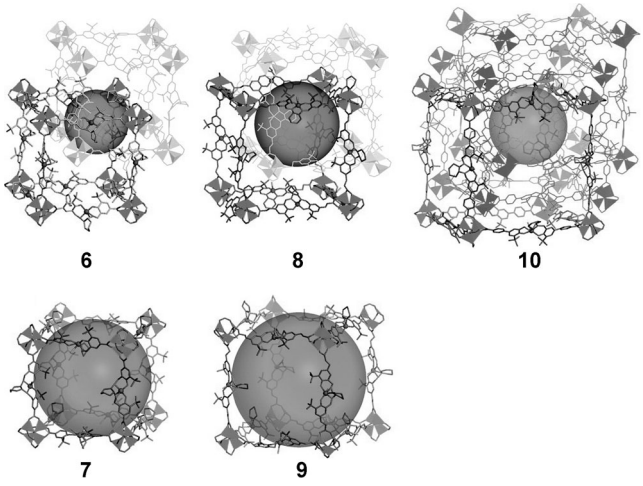

Figure 8. Variety of interpenetrations and cavity sizes (in parentheses) for **6** (1.4 nm), **7** (2.6 nm), **8** (2.0 nm), **9** (3.2 nm), and **10** (1.8 nm). Reproduced with permission from Ref. [15].

effective in catalyzing enantioselective epoxidation of a variety of unfunctionalized alkenes with up to 92% *ee*. The rate of conversion was in the increasing order of **6** > **10** > **8** > **7** > **9**, which is in consistent with the increasing order of the channel sizes. It has been shown that the reaction rate for the interpenetrated M′MOFs depends upon the diffusion rate of alkenes, oxidants, and the final epoxide products into the small open channels. For the case of non-interpenetrated M′MOFs (i.e. with larger open channels), the rate-determining step is limited by intrinsic activity of the catalytic molecular building blocks.

A series of chiral M′MOFs constructed by postsynthetic modification were also prepared for the highly enantioselective asymmetric addition of diethylzinc and/or alkynyl zinc to aldehydes.[16] In these examples of chiral M′MOFs, the chiral organic linkers (*R*)-6,6′-dichloro-2,2′-dihydroxy-1,1-binaphthyl-4,4′-bipyridine or binol-derived tetracarboxylic acid were employed to construct homochiral MOFs, while the Lewis acidic Ti^{4+} catalytic sites were immobilized on the chiral pore surfaces by the postsynthetic reaction of $Ti(OiPr)_4$ with the phenol functional groups.

5. Functional M′MOFs as Chemical Sensors

Xie et al. successfully incorporated highly phosphorescent metalloligands H_3L^5 and H_3L^6 into M′MOFs $[Zn_4(\mu^4$-

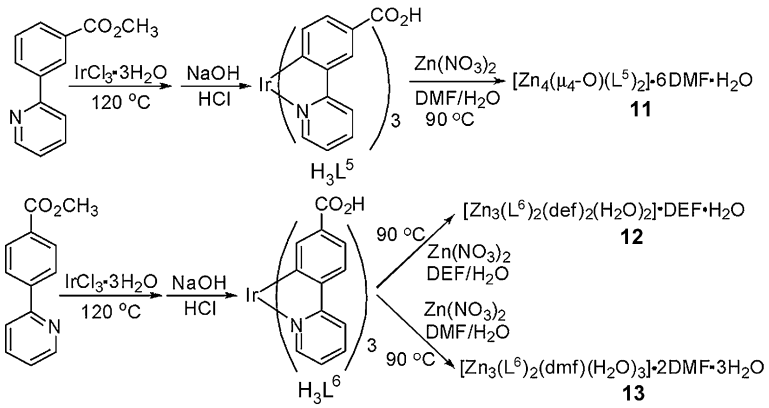

Scheme 5. Synthesis of three M′MOFs and the metalloligands H_3L^5 and H_3L^6 of tricarboxylate derivatives of $[Ir(ppy)_3]$. Reproduced with permission from Ref. [17].

$O)(L^5)_2]\cdot 6DMF\cdot H_2O$ (**11**), $[Zn_3(L^6)_2(def)_2(H_2O)_2]\cdot DEF\cdot H_2O$ (**12**) and $[Zn_3(L^6)_2(dmf)(H_2O)_3]\cdot 2DMF\cdot 3H_2O$ (**13**) for chemical sensors (Scheme 5).[17] While the permanent porosity of **11** was confirmed by N_2 and CO_2 sorption measurements, **12** and **13** were nonporous. The most significant observation was molecular O_2 sensing with quenching efficiencies of 59, 41, 32, 16, and 8% for **11**, **12**, **13**, H_3L^5 and H_3L^6 respectively. The Stern–Volmer plot revealed that intensity of **11** dropped to a stable value after each O_2 dose (Figure 9a), and the luminescence was reversibly quenched by molecular O_2 (Figure 9b) after varying cycles of O_2 exposure and removal. In contrast, little irreversible quenching was observed for the two nonporous materials. Thus, efficient and reversible luminescence quenching for the microporous M′MOF material suggested the necessity of fast diffusion of O_2 through the open pores.

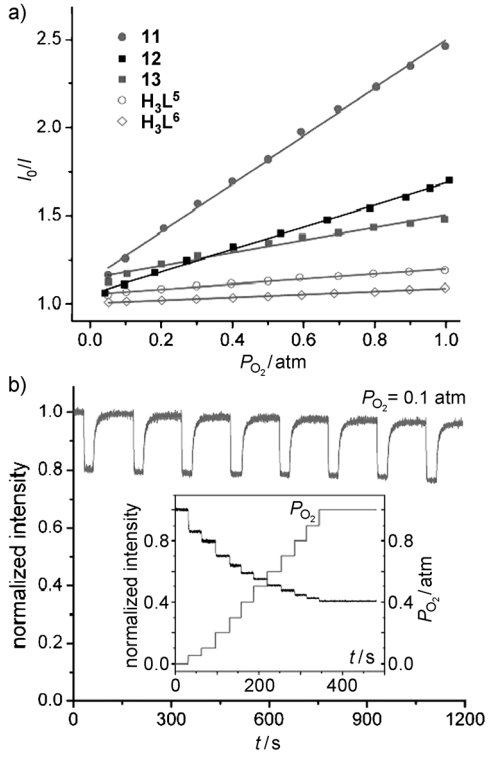

Figure 9. a) Stern–Volmer plot showing I_0/I versus O_2 partial pressure for iridium complexes H_3L^5 and H_3L^6 and M′MOFs **11**–**13**. b) Reversible quenching of phosphorescence of **11** upon alternating exposure to 0.1 atm O_2 and application of vacuum. The inset shows rapid equilibration of phosphorescence of **11** after each dose of O_2. Reproduced with permission from Ref. [17].

6. Functional M′MOFs as Photoactive Materials

Chandler et al. used luminescent metalloligands $[Ln(L^7)_4]^{5-}$ (L^7 = 4,4′-disulfo-2,2′-bipyridine-*N*,*N*′-dioxide) to construct 3D M′MOFs with open channels: $[\{Na_6(H_2O)_6\}\{Ln(L^7)_4\}(H_2O)_nCl]$ and $[Ba_2(H_2O)_4\{Ln(L^7)_3(H_2O)_2\}(H_2O)_nCl]$ where Ln = Sm^{3+}, Eu^{3+}, Gd^{3+}, Tb^{3+}, Dy^{3+} (Scheme 6).[18] Although these structures contracted upon solvent removal, some of the new solids were microporous, as shown by CO_2, N_2 and water vapor sorption isotherms. The Ln ions with the exception of Gd^{3+} could be sensitized by the receiver ligand. It was found that luminescence lifetimes depend on hydration and other guests in the channels of the solids.

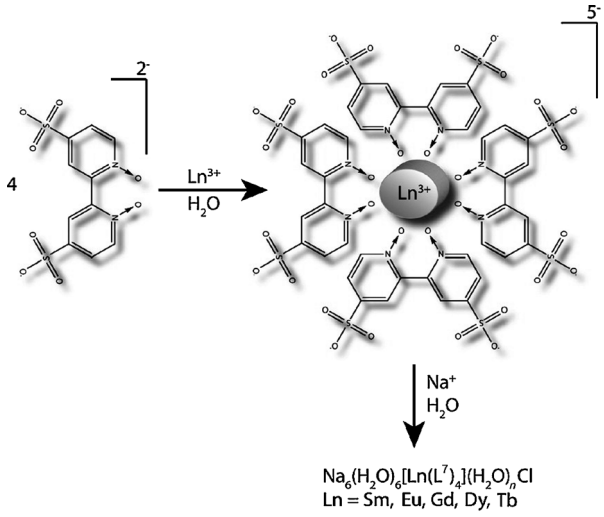

Scheme 6. Construction of luminescent microporous mixed Ln/Na organic frameworks. Reproduced with permission from Ref. [18].

It would be very interesting to see the photophysical and photochemical properties of photoactive species within a confined M′MOF environment. Blake et al. successfully immobilized photoactive metalloligands [M(2,2′-bipyridine)-$(CO)_3X$] (M = Re, Mn; X = Br, Cl) to connect Mn^{II} cations as nodes to form three M′MOFs (**14**: $[\{MnC_{12}H_6N_2O_4(dmf)_2Re(CO)_3Cl\}_\infty]$; **15**: $[\{MnC_{12}H_6N_2O_4(dmf)_2Mn(CO)_3Br\}_\infty]$, **15a**: $[\{MnC_{12}H_6N_2O_4(dmf)_2Mn(CO)_3Cl\}_\infty]$).[19] The X-ray crystal structure of **14** revealed the presence of a *fac* arrangement of the metalloligand (Figure 10a) and manganese carboxylate chains along the *a* axis. These chains were interconnected by the metalloligands to form a 3D framework (Figure 10b) of platinum sulfide topology. Compound **14** exhibited excited-state formation as a result of intraligand charge transfer (π–π*). The π–π* excited states appeared to be lower in energy than metal-to-ligand charge-transfer (MLCT) states within the restricted M′MOF environment, which is an extraordinary phenomenon. Compound **14** lost CO and underwent *fac* to *mer* photochemical conversion upon UV irradiation. Solid-state powder attenuated total reflectance infrared (ATR-IR) measurement of **15** before and after UV photolysis showed a high conversion of approximately 25% of the *fac* to the *mer* isomer. A similar type of photochemical conversion was also observed for **15a**, as evident from a single-crystal XRD study (Figure 10c,d). These studies opened up a new possibility to use M′MOFs as hosts to stabilize typically short-lived species and give further insight into the nature of short-lived intermediates.

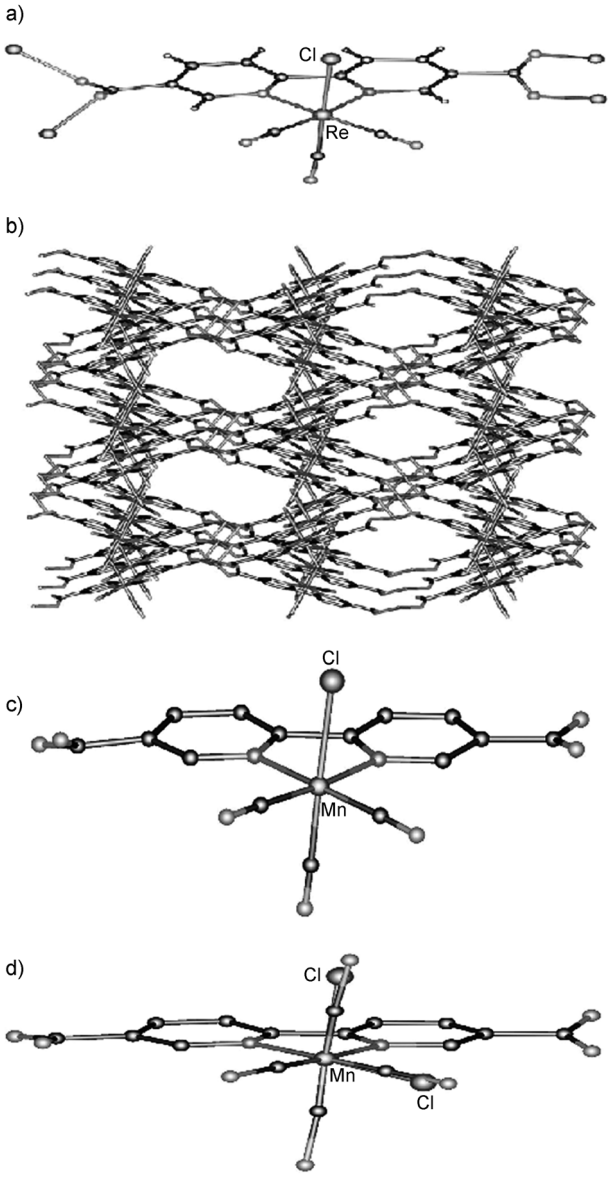

Figure 10. a) View of the {Re(diimine)$(CO)_3$Cl} moiety confirming the *fac* configuration in **14**. b) View of the three-dimensional framework formed by **14**, indicating the interlinking of {Mn(carboxylate)}$_\infty$ chains by {Re(diimine)$(CO)_3$Cl} moieties. c) The {Mn(diimine)$(CO)_3$Cl} moiety for **15a** with chloride occupancy only in the axial sites, confirming the *fac* configuration. d) Structure **15b** reveals chloride occupancy (30%) in the equatorial positions, confirming that a portion of the {Mn(diimine)$(CO)_3$Cl} moieties adopt the *mer* arrangement. Reproduced with permission from Ref. [19].

Kent et al. reported M′MOFs to study Ru→Os energy-transfer process that have potential application in light-harvesting materials.[20] The M′MOFs with 0.3, 0.6, 1.4, and 2.6 mol% Os doping were also synthesized to study the energy-transfer dynamics with two-photon excitation at 850 nm. It was found that the Ru lifetime at 620 nm decreased from 171 ns in the pure Ru MOF to 29 ns in the sample with 2.6 mol% Os doping, with an initial growth in Os emission corresponding to the rate of decay of the Ru excited state (Figure 11).

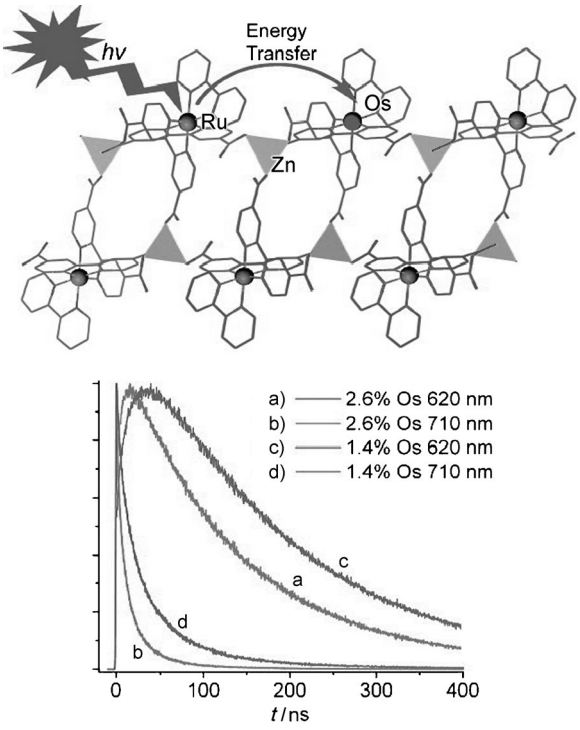

Figure 11. Top: X-ray crystal structure of the L_{Ru}Zn M′MOF showing the side view of a 2D bilayer along the *b* axis and energy transfer from Ru to Os. Bottom: Transients for 1.4 and 2.6 mol% Os-doped L_{Ru}Zn M′MOFs at 620 and 710 nm with emission at 620 nm dominated by Ru^{II}* and at 710 nm by Os^{II}*. Reproduced with permission from Ref. [20].

7. Nanoscale M′MOFs for Drug Delivery and Biomedical Imaging

Micrometer- and nanometer-sized particles are very important because of their potential applications in several fields, including catalysis, optics, biosensing, and data storage.[28–31] Rieter et al. reported Pt-containing nanoscale M′MOF $[Tb_2(dscp)_3(H_2O)_{12}]$ (**16;** dscp = disuccinatocisplatin) with a diameter of (58.3 ± 11.3) nm for potential application in anticancer drug delivery.[29] The silica-coated particles **16′** exhibited longer half-lives for dscp release from the particles ($t_{1/2} \approx 5.5$ h for **16′a** with 2 nm silica coating, $t_{1/2} \approx 9$ h for **16′b** with 7 nm silica coating, and $t_{1/2} \approx 1$ h for as-synthesized **16**). In vitro cancer cell cytotoxicity assays with HT-29 human cells showed that internalized **16′** particles readily released the dscp moieties, thus establishing the anticancer efficiency of these silica-coated particles.

Liu et al. reported phosphorescent nanoscale M′MOFs **17** (Zn^{2+}) and **18** (Zr^{4+}) constructed from metalloligand [Ru-{5,5′-$(OOC)_2$bpy}$(bpy)_2$] (bpy = 2,2′-bipyridine) and Zn^{2+}/Zr^{4+} salts, which exhibited high dye loadings of 78.7 and 57.4%, respectively.[30] Compound **18** was stable in water but rapidly decomposed in phosphate-buffered saline (PBS) at 37 °C with a half-life of about 0.5 h. To slow down the release of dye molecules in biologically relevant media, particles of **18** were coated with a thin shell of silica to get SiO_2@**18** particles, which have a longer half life of 3.2 h. To prevent particle aggregation, increase the dispersibility of nanoparticles, and target certain biomarkers, SiO_2@**18** particles were further coated with $CH_3OPEG2000\text{-}Si(OEt)_3$ and anisamide-$PEG2000\text{-}Si(OEt)_3$ to afford PEGylated and targeted particles, PEG-SiO_2@**18** and AA-PEG-SiO_2@**18** (PEG = poly(ethylene glycol), AA = anisamide), respectively. The nanoscale coordination polymers (NCPs) were tested for their potential usage as contrast agents for optical imaging. H460 lung cancer cells were incubated with PEG-SiO_2@**18** and AA-PEG-SiO_2@**18** particles for 24 h, and no appreciable cell death was observed (Figure 12d). Confocal fluorescence microscopy studies (Figure 12a–c) revealed significant MLCT luminescent signal when H460 cells were incubated with AA-PEG-SiO_2@**18** particles. In contrast, less luminescence intensity was observed for the nontargeted PEG-SiO_2@**18** particles. Furthermore, enhanced dye uptake was observed for AA-PEG-SiO_2@**18** (Figure 12e) particles in comparison with either **18** or PEG-SiO_2@**18** particles.

8. Conclusion and Outlook

Construction of functional mixed metal–organic frameworks (M′MOFs) is still in an early stage. The bright promise of this new metalloligand approach to assemble M′MOF materials with functional sites for the recognition of small molecules will initiate extensive research on the exploration and discovery of new functional M′MOF materials. It is foreseen that a variety of novel M′MOFs will be realized for applications in gas storage and separation, enantioselective

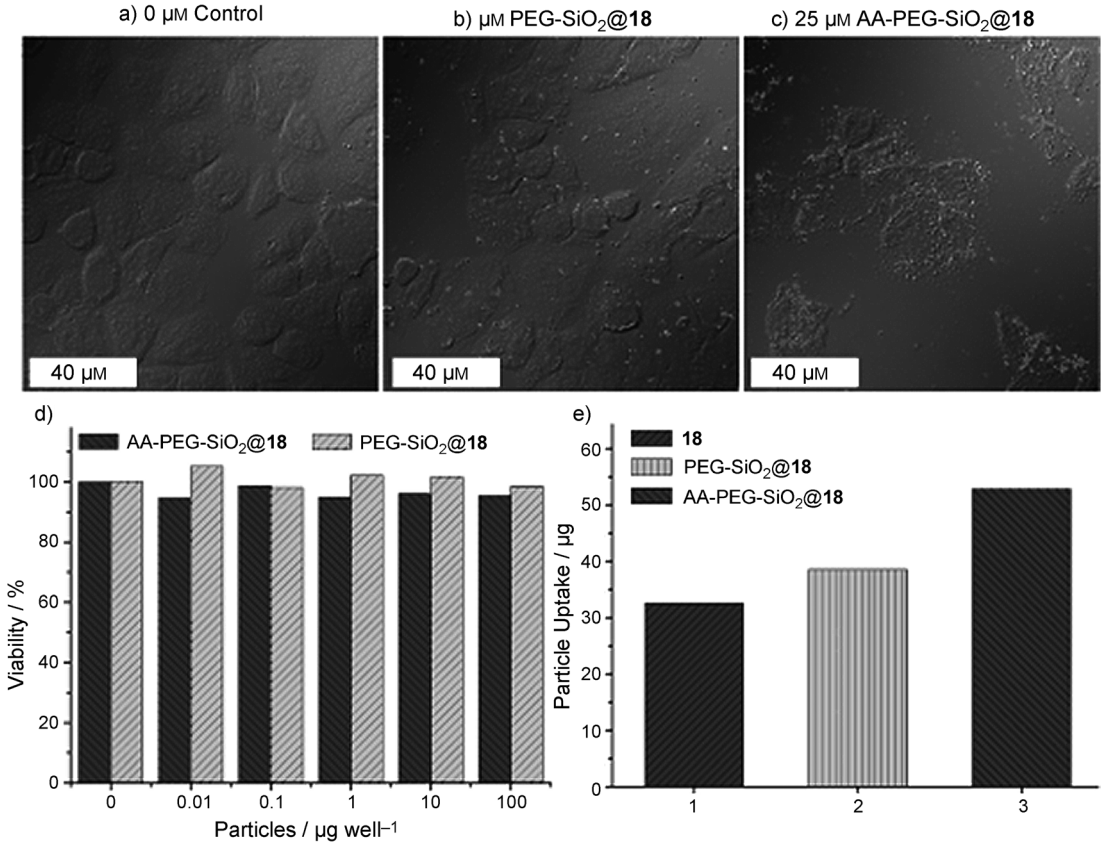

Figure 12. Confocal fluorescence microscopy images of H460 lung cancer cells incubated a) without any particles, b) with PEG-SiO_2@**18** particles, and c) with AA-PEG-SiO_2@**18** particles. d) In vitro viability assay for H460 cells incubated with various amounts of PEG-SiO_2@**18** and AA-PEG-SiO_2@**18** particles. e) Particle uptake studies in H460 cells. Reproduced with permission from Ref. [30].

separation, heterogeneous catalysis, sensing, and as photoactive and nanoscale drug delivery and biomedical imaging materials in the near future.

We gratefully acknowledge the financial support of awards from the NSF (CHE 0718281) and the Welch Foundation (AX-1730, B.C.).

Received: March 2, 2011
Revised: May 19, 2011
Published online: September 16, 2011

[1] a) S. Kitagawa, R. Kitaura, S. I. Noro, *Angew. Chem.* **2004**, *116*, 2388; *Angew. Chem. Int. Ed.* **2004**, *43*, 2334; b) O. M. Yaghi, M. O'Keeffe, N. W. Ockwig, H. K. Chae, M. Eddaoudi, J. Kim, *Nature* **2003**, *423*, 705; c) J. J. Perry IV, J. A. Perman, M. J. Zaworotko, *Chem. Soc. Rev.* **2009**, *38*, 1400; d) N. W. Ockwig, O. Delgado-Friedrichs, M. O'Keeffe, O. M. Yaghi, *Acc. Chem. Res.* **2005**, *38*, 176; e) K. S. Suslick, P. Bhyrappa, J.-H. Chou, M. E. Kosal, S. Nakagaki, D. W. Smithenry, S. R. Wilson, *Acc. Chem. Res.* **2005**, *38*, 283; f) L. Ma, C. Abney, W. Lin, *Chem. Soc. Rev.* **2009**, *38*, 1248; g) O. K. Farha, J. T. Hupp, *Acc. Chem. Res.* **2010**, *43*, 1166; h) G. Férey, C. Serre, *Chem. Soc. Rev.* **2009**, *38*, 1380; i) L. J. Murray, M. Dinca, J. R. Long, *Chem. Soc. Rev.* **2009**, *38*, 1294; j) W. Lin, W. J. Rieter, K. M. L. Taylor, *Angew. Chem.* **2009**, *121*, 660; *Angew. Chem. Int. Ed.* **2009**, *48*, 650; k) J. Li, R. J. Kuppler, H.-C. Zhou, *Chem. Soc. Rev.* **2009**, *38*, 1477; l) Z. Wang, S. M. Cohen, *Chem. Soc. Rev.* **2009**, *38*, 1315; m) T. Dueren, Y.-S. Bae, R. Q. Snurr, *Chem. Soc. Rev.* **2009**, *38*, 1237; n) H.-L. Jiang, Q. Xu, *Chem. Commun.* **2011**, *47*, 3351; o) G. K. H. Shimizu, R. Vaidhyanathan, J. M. Taylor, *Chem. Soc. Rev.* **2009**, *38*, 1430; p) S. R. Caskey, A. G. Wong-Foy, A. J. Matzger, *J. Am. Chem. Soc.* **2008**, *130*, 10870; q) R. E. Morris, P. S. Wheatley, *Angew. Chem.* **2008**, *120*, 5044; *Angew. Chem. Int. Ed.* **2008**, *47*, 4966; r) X. Zhao, B. Xiao, A. J. Fletcher, K. M. Thomas, D. Bradshaw, M. J. Rosseinsky, *Science* **2004**, *306*, 1012; s) L. Pan, D. H. Olson, L. R. Ciemnolonski, R. Heddy, J. Li, *Angew. Chem.* **2006**, *118*, 632; *Angew. Chem. Int. Ed.* **2006**, *45*, 616; t) S. Yang, X. Lin, A. J. Blake, G. S. Walker, P. Hubberstey, N. R. Champness, M. Schröder, *Nat. Chem.* **2009**, *1*, 487; u) An, S. J. Geib, N. L. Rosi, *J. Am. Chem. Soc.* **2010**, *132*, 38; v) J. Zhang, J. Bu, S. Chen, T. Wu, S. Zheng, Y. Chen, R. Nieto, P. Feng, X. Bu, *Angew. Chem.* **2010**, *122*, 9060; *Angew. Chem. Int. Ed.* **2010**, *49*, 8876; w) J.-P. Zhang, X.-M. Chen, *J. Am. Chem. Soc.* **2009**, *131*, 5516; x) M. C. Das, P. K. Bharadwaj, *J. Am. Chem. Soc.* **2009**, *131*, 10942; y) J. S. Seo, D. Whang, H. Lee, S. I. Jun, J. Oh, Y. J. Jeon, K. Kim, *Nature* **2000**, *404*, 982; z) B. Chen, S. C. Xiang, G. Qian, *Acc. Chem. Res.* **2010**, *43*, 1115.

[2] M. Eddaoudi, J. Kim, N. L. Rosi, D. T. Vodak, J. Wachter, M. O'Keeffe, O. M. Yaghi, *Science* **2002**, *295*, 469.

[3] R. Vaidhyanathan, S. S. Iremonger, K. W. Dawson, G. K. H. Shimizu, *Chem. Commun.* **2009**, 5230; R. Vaidhyanathan, S. S. Iremonger, G. K. H. Shimizu, P. G. Boyd, S. Alavi, T. K. Woo, *Science* **2010**, *330*, 650.

[4] B. F. Abrahams, B. F. Hoskins, D. M. Michail, R. Robson, *Nature* **1994**, *369*, 727.

[5] a) Y. Pei, M. Verdaguer, O. Kahn, J. Sletten, J. P. Renard, *J. Am. Chem. Soc.* **1986**, *108*, 7428; b) O. Kahn, *Acc. Chem. Res.* **2000**, *33*, 647.

[6] M. E. Kosal, J.-H. Chou, S. R. Wilson, K. S. Suslick, *Nat. Mater.* **2002**, *1*, 118.

[7] a) A. Hu, H. L. Ngo, W. Lin, *Angew. Chem.* **2003**, *115*, 6182; *Angew. Chem. Int. Ed.* **2003**, *42*, 6000; b) A. Hu, H. L. Ngo, W. Lin, *J. Am. Chem. Soc.* **2003**, *125*, 11490.

[8] a) R. Kitaura, G. Onoyama, H. Sakamoto, R. Matsuda, S. Noro, S. Kitagawa, *Angew. Chem.* **2004**, *116*, 2738; *Angew. Chem. Int. Ed.* **2004**, *43*, 2684; b) H. Sakamoto, R. Matsuda, S. Bureekaew, D. Tanaka, S. Kitagawa, *Chem. Eur. J.* **2009**, *15*, 4985.

[9] B. Chen, F. R. Fronczek, A. W. Maverick, *Inorg. Chem.* **2004**, *43*, 8209.

[10] B. Chen, X. Zhao, A. Putkham, K. Hong, E. B. Lobkovsky, E. J. Hurtado, A. J. Fletcher, K. M. Thomas, *J. Am. Chem. Soc.* **2008**, *130*, 6411.

[11] S. Xiang, Z. Zhang, C.-G. Zhao, K. Hong, X. Zhao, D.-R. Ding, M.-H. Xie, C.-D. Wu, M. C. Das, R. Gill, K. M. Thomas, B. Chen, *Nat. Commun.* **2011**, *2*, 204.

[12] E. D. Bloch, D. Britt, C. Lee, C. J. Doonan, F. J. Uribe-Romo, H. Furukawa, J. R. Long, O. M. Yaghi, *J. Am. Chem. Soc.* **2010**, *132*, 14382.

[13] G. Yuan, C. Zhu, W. Xuan, Y. Cui, *Chem. Eur. J.* **2009**, *15*, 6428.

[14] S.-H. Cho, B. Ma, S. T. Nguyen, J. T. Hupp, T. E. Albrecht-Schmitt, *Chem. Commun.* **2006**, 2563.

[15] F. Song, C. Wang, J. M. Falkowski, L. Ma, W. Lin, *J. Am. Chem. Soc.* **2010**, *132*, 15390.

[16] a) C.-D. Wu, A. Hu, L. Zhang, W. Lin, *J. Am. Chem. Soc.* **2005**, *127*, 8940; b) C.-D. Wu, W. Lin, *Angew. Chem.* **2007**, *119*, 1093; *Angew. Chem. Int. Ed.* **2007**, *46*, 1075; c) L. Ma, J. M. Falkowski, C. Abney, W. Lin, *Nat. Chem.* **2010**, *2*, 838; d) L. Ma, C.-D. Wu, M. M. Wanderley, W. Lin, *Angew. Chem.* **2010**, *122*, 8420; *Angew. Chem. Int. Ed.* **2010**, *49*, 8244.

[17] Z. Xie, L. Ma, K. E. deKrafft, A. Jin, W. Lin, *J. Am. Chem. Soc.* **2010**, *132*, 922.

[18] a) B. D. Chandler, D. T. Cramb, G. K. H. Shimizu, *J. Am. Chem. Soc.* **2006**, *128*, 10403; b) B. D. Chandler, A. P. Côté, D. T. Cramb, J. M. Hill, G. K. H. Shimizu, *Chem. Commun.* **2002**, 1900; c) B. D. Chandler, J. O. Yu, D. T. Cramb, G. K. H. Shimizu, *Chem. Mater.* **2007**, *19*, 4467.

[19] A. J. Blake, N. R. Champness, T. L. Easun, D. R. Allan, H. Nowell, M. W. George, J. Jia, X.-Z. Sun, *Nat. Chem.* **2010**, *2*, 688.

[20] C. A. Kent, B. P. Mehl, L. Ma, J. M. Papanikolas, T. J. Meyer, W. Li, *J. Am. Chem. Soc.* **2010**, *132*, 12767.

[21] D. W. Smithenry, S. R. Wilson, K. S. Suslick, *Inorg. Chem.* **2003**, *42*, 7719.

[22] J.-P. Lang, Q.-F. Xu, R.-X. Yuan, B. F. Abrahams, *Angew. Chem.* **2004**, *116*, 4845; *Angew. Chem. Int. Ed.* **2004**, *43*, 4741.

[23] S. R. Halper, L. Do, J. R. Stork, S. M. Cohen, *J. Am. Chem. Soc.* **2006**, *128*, 15255.

[24] S. Kitagawa, S.-I. Noro, T. Nakamura, *Chem. Commun.* **2006**, 701.

[25] Y. Zhang, B. Chen, F. R. Fronczek, A. W. Maverick, *Inorg. Chem.* **2008**, *47*, 4433.

[26] E.-Y. Choi, P. M. Barron, R. W. Novotny, H.-T. Son, C. Hu, W. Choe, *CrystEngComm* **2009**, *11*, 553.

[27] M.-H. Xie, X.-L. Yang, C.-D. Wu, *Chem. Commun.* **2011**, *47*, 5521.

[28] See Ref. [1j].

[29] W. J. Rieter, K. M. Pott, K. M. L. Taylor, W. Lin, *J. Am. Chem. Soc.* **2008**, *130*, 11584.

[30] D. Liu, R. C. Huxford, W. Lin, *Angew. Chem.* **2011**, *123*, 3780; *Angew. Chem. Int. Ed.* **2011**, *50*, 3696.

[31] a) M. Oh, C. A. Mirkin, *Nature* **2005**, *438*, 651; b) M. Oh, C. A. Mirkin, *Angew. Chem.* **2006**, *118*, 5618; *Angew. Chem. Int. Ed.* **2006**, *45*, 5492; c) Y.-M. Jeon, J. Heo, C. A. Mirkin, *J. Am. Chem. Soc.* **2007**, *129*, 7480.

[32] J. J. M. Beenakker, V. D. Borman, S. Y. Krylov, *Chem. Phys. Lett.* **1995**, *232*, 379.

[33] R. Noyori, *Angew. Chem.* **2002**, *114*, 2108–2123; *Angew. Chem. Int. Ed.* **2002**, *41*, 2008–2022 and references therein.

[34] BET surface areas are more meaningful than Langmuir ones in MOFs and related materials, see T. Dueren, F. Millange, G. Ferey, K. S. Walton, R. Q. Snurr, *J. Phys. Chem. C* **2007**, *111*, 15350.

